Commun. Comput. Phys.
doi: 10.4208/cicp.120615.090516a

Vol. **20**, No. 4, pp. 969-988
October 2016

Scale Transitions in Magnetisation Dynamics

Mikhail Poluektov[1,*], Olle Eriksson[2] and Gunilla Kreiss[1]

[1] *Department of Information Technology, Uppsala University, Box 337, SE-751 05 Uppsala, Sweden.*
[2] *Department of Physics and Astronomy, Uppsala University, Box 516, SE-751 05 Uppsala, Sweden.*

Received 12 June 2015; Accepted (in revised version) 9 May 2016

Abstract. Multiscale modelling is a powerful technique, which allows for computational efficiency while retaining small-scale details when they are essential for understanding a finer behaviour of the studied system. In the case of materials modelling, one of the effective multiscaling concepts is domain partitioning, which implies the existence of an explicit interface between various material descriptions, for instance atomistic and continuum regions. When dynamic material behaviour is considered, the major problem for this technique is dealing with reflections of high frequency waves from the interface separating two scales. In this article, a new method is suggested, which overcomes this problem for the case of magnetisation dynamics. The introduction of a damping band at the interface between scales, which absorbs high frequency waves, is suggested. The idea is verified using a number of one-dimensional examples with fine/coarse scale discretisation of a continuum problem of spin wave propagation. This work is the first step towards establishing a reliable atomistic/continuum multiscale transition for the description of the evolution of magnetic properties of ferromagnets.

AMS subject classifications: 65M55, 65Z05, 37M05

PACS: 75.30.Ds, 75.78.Cd

Key words: Magnetisation dynamics, spin waves, multiscale modelling, multigrid methods.

1 Introduction

Experimental investigations of the magnetisation dynamics is currently a most active and challenging research field [1–6]. The scientific questions which are addressed in these studies focus e.g. on advanced magnetic materials for data storage and magnetic memories, with the aim of understanding the fundamental limit of magnetisation switching and reversal. Technical avenues to reach this fundamental limit are pursued experimentally, e.g. using optical control, current induced phenomena and all-thermal switching,

*Corresponding author. *Email addresses:* mikhail.poluektov@it.uu.se (M. Poluektov), olle.eriksson@physics.uu.se (O. Eriksson), gunilla.kreiss@it.uu.se (G. Kreiss)

 ©2016 Global-Science Press

https://doi.org/10.4208/cicp.120615.090516a Published online by Cambridge University Press

and several breakthroughs have been reported. In these experimental works it has been found that a Laser pulse can be used to demagnetise a ferromagnetic sample on time scales of picoseconds down to femtoseconds [1–6]. These studies are still on a very fundamental level and for practical aspects it can be argued that in device design a setup involving a Laser might be a hinder.

On the theory side methodologies have been developed that are based on the concept of micromagnetism [7,8], which provides a framework for understanding magnetisation dynamics on length scales of micrometers and in which the magnetisation is considered as a continuum variable. In this approach, the magnetism is treated as a continuum vector field on a relatively large length scale. The power of being able to couple such continuum based theories to the recently emerging atomistic theory of magnetisation dynamics [9] is obvious. One could then treat larger sections of the simulation box that have less structure or detail using the continuum model, while smaller regions with more detail could be treated on an atomistic scale. However, it is not straightforward to take the necessary step in this multiscale approach to magnetisation dynamics. Nevertheless, a reliable theoretical tool which could serve as a complement to modern experimental works on magnetisation dynamics and ultrafast switching phenomena is highly desirable, both when it comes to understanding the mechanisms which play role, but also for predicting phenomena and novel materials/concepts.

There are multiple ways of performing multiscale simulations, one of which is domain partitioning, where there is an explicit interface between various material descriptions. Models of coupling atomistic and continuum descriptions were initially developed to describe the mechanical behaviour of solids [10]. There is a wide variety of methods, which are applicable in the case of quasistatic behaviour [11], however, modelling the dynamic behaviour is more problematic, in particular, wave reflections from the interface between two descriptions present a challenge for multiscale techniques. Recently a significant progress has been made in this area [12,13]; a modification of the equation of motion of atoms in the proximity of the atomistic/continuum interface was suggested, such that high frequency waves are damped in this region.

There are also multiscale techniques, which are developed for the simulation of the magnetic material properties. In [14], some aspects of constructing continuum micromagnetic description and estimating its parameters based on atomistic spin dynamics were discussed. In [15], a way of coarse-graining from the atomistic to micromagnetic description, with a gradual transition of discretisation between descriptions, was presented. However, the proposed method was limited to the static problem of finding equilibrium states in the domain partitioned into atomistic and micromagnetic regions. Recently a way of constructing a transition between two descriptions for dynamic problems was published [16]. This approach suggested an overlapping of the atomistic and the continuum regions where the exchange energies of the two models are mixed. The model was used to describe the dynamics of Bloch points, which were surrounded by the atomistic description, while the rest of the material was modelled as a continuum. However, the continuum model still had to be discretised down to the atomistic scale,

https://doi.org/10.4208/cicp.120615.090516a Published online by Cambridge University Press

which limits the gain in efficiency.

The aim of this work is to investigate a way of interfacing two scales, where both fine scale and coarse scale regions are represented by the continuum description and where a sharp transition between scales might exist. Although the scope of this article is limited to the use of the continuum description at the fine scale as well, the proposed coupling method is designed to be valid also when the atomistic description is adopted at the fine scale, since the discrete equations from the well-resolved continuum description are of the same type as the atomistic description. As outlined above, when dynamic systems are considered, the major problem for multiscale methods is dealing with reflections of high frequency waves from the interface separating two scales. Domain partitioning into coarse and fine regions, where the latter isolates the source of waves or a heterogeneity in the material, implies that such high frequency waves are significant only in the fine region and are neglected in the coarse region. The justification of this disregard originates from the fact that for systems with physical damping, high frequency waves are attenuated faster than low frequency waves and have a limited range. Therefore, to avoid wave reflections from the interface in the partitioned domain, high frequency waves have to be damped at the interface.

There are methods of wave absorption at the boundaries for PDEs, such as the Perfectly Matched Layer (PML) technique. However, these methods rely heavily on the specific form of the PDE to which they are applied and modification of the underlying PDE requires re-derivation of the PML terms. Moreover, such methods were initially developed for linear PDEs and it is known, that application of these methods to non-linear cases often leads to non-linear instabilities. In the current study, the proposed method should be applicable not only for the continuum case, but also for the atomistic case and has to remain valid when the governing equations are extended with various additional terms modifying the material description. Therefore, a relatively simple, but robust, absorbing layer (damping band) is proposed here and its numerical efficiency is investigated in detail.

In this article, the modification of the Landau-Lifshitz equation in the vicinity of the interface is proposed, thereby introducing a damping band that absorbs high frequency waves, based on the idea of [12]. To investigate the behaviour of the introduced damping layer, a one-dimensional domain is considered, which is illustrated in Fig. 1b. In Section 2, the modification of the Landau-Lifshitz equation is discussed and a particular case of small-amplitude spin waves (Fig. 1a) is analysed analytically. In Section 3, propagation of spin waves, which are generated in the fine scale, and of wave packets resulting from heterogeneities in the initial conditions is investigated computationally.

2 Methods

The dynamics of volume-averaged magnetisation in the case of a one-dimensional domain and absence of physical damping is described by the following equation [7]:

https://doi.org/10.4208/cicp.120615.090516a Published online by Cambridge University Press

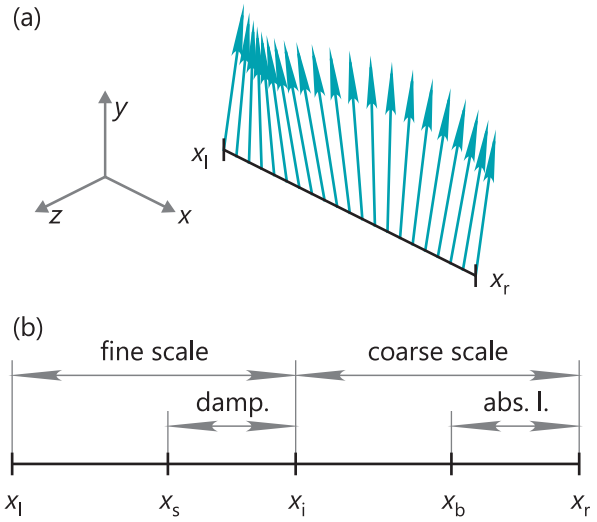


Figure 1: Schematic representation of spin wave in a one-dimensional domain (a) and the separation of the domain into different regions, where the coarse scale is represented by the continuum model and the fine scale is represented by either atomistic or continuum description (b). In the fine-scale region, additional damping is introduced near the interface. In the coarse-scale region, the absorbing layer near the right boundary is added to avoid wave reflections from the boundary (only in some computational examples in this article).

$$\frac{\partial}{\partial t}\vec{m} = -\beta_L \vec{m} \times \frac{\partial^2}{\partial x^2}\vec{m}, \quad x \in [x_l; x_s] \cup [x_i; x_r], \tag{2.1}$$

where $\vec{m}$ is the normalised magnetisation, such that $|\vec{m}| = 1$, and β_L is a scaled gyromagnetic ratio[†]. Note that $\vec{m}$ is a three dimensional vector, albeit with a one-dimensional argument, x. The domain $x_l \le x \le x_r$ is considered to be split in two sub-domains with the interface at $x = x_i$ (see Fig. 1). In the region adjoining the interface, $x_s < x < x_i$, an additional damping is introduced into the equation describing the magnetisation dynamics:

$$\frac{\partial}{\partial t}\vec{m} = -\beta_L \vec{m} \times \frac{\partial^2}{\partial x^2}\vec{m} - \gamma_D \vec{m} \times (\vec{m} \times \vec{m}_A), \quad x \in (x_s; x_i), \tag{2.2}$$

where γ_D is the strength of the damping inside the damping zone and $\vec{m}_A$ is an average of the magnetisation over a certain region. Note that $\vec{m}$ and $\vec{m}_A$ are in general not parallel, and that both are functions of x. The last term in the Eq. (2.2) "forces" $\vec{m}$ and $\vec{m}_A$ to become parallel acting effectively as a low-pass filter. The detailed expressions for γ_D and $\vec{m}_A$ are given in Section 2.4, following the analysis of special cases of small amplitude spin wave propagation (Section 2.2) and, in particular, high frequency waves (Section 2.3). Although the selection of the damping method is based on the example of stationary spin waves with small amplitude, it is computationally shown that such a damping zone

[†]In this article, emphasis is made on the numerical technique, therefore all quantities, including x and t, are considered to be dimensionless, which is common in numerical analysis [17]. This nondimensionalisation is performed by scaling parameter β_L.

https://doi.org/10.4208/cicp.120615.090516a Published online by Cambridge University Press

works well in other cases (see Section 3). Parameters x_l, x_s, x_i and x_r (see Fig. 1) are only introduced for descriptive purposes. In the subsequent sections, the width of the damping zone, s, is used. In the next section, Eqs. (2.1) and (2.2) are re-written in terms of two angles, θ and ϕ, which is convenient for the analysis of spin waves.

Although the separation of the domain into the fine scale and the coarse scale regions has already been mentioned, the actual discretisation is introduced in Section 3.2, where numerical examples are discussed. The domains are assumed to be strongly coupled, i.e. the interface point (x_i) is the right boundary for the fine scale domain and the left boundary for the coarse scale domain.

2.1 Spin waves

To analyse the propagation of the spin waves through the domain, $\vec{m}$ is represented through two angles:

$$\vec{m}=\vec{e}_x\sin\theta\cos\phi+\vec{e}_y\cos\theta+\vec{e}_z\sin\theta\sin\phi, \tag{2.3}$$

where θ is the amplitude of the spin wave and ϕ is the phase. When the expression for $\vec{m}$ in the form of (2.3) is substituted into (2.1) and (2.2), the following equations for the amplitude and the phase are obtained:

$$\frac{\partial\theta}{\partial t}=-2\beta_\mathrm{L}\frac{\partial\theta}{\partial x}\frac{\partial\phi}{\partial x}\cos\theta-\beta_\mathrm{L}\frac{\partial^2\phi}{\partial x^2}\sin\theta+\Gamma_\theta, \tag{2.4}$$

$$\frac{\partial\phi}{\partial t}\sin\theta=-\beta_\mathrm{L}\left(\frac{\partial\phi}{\partial x}\right)^2\sin\theta\cos\theta+\beta_\mathrm{L}\frac{\partial^2\theta}{\partial x^2}-\Gamma_\phi, \tag{2.5}$$

$$\Gamma_\theta=\begin{cases}\gamma_\mathrm{D}\left(m_{\mathrm{A}x}\cos\theta\cos\phi-m_{\mathrm{A}y}\sin\theta+m_{\mathrm{A}z}\cos\theta\sin\phi\right), & x\in(x_\mathrm{s};x_\mathrm{i}),\\ 0, & x\in[x_\mathrm{l};x_\mathrm{s}]\cup[x_\mathrm{i};x_\mathrm{r}],\end{cases} \tag{2.6}$$

$$\Gamma_\phi=\begin{cases}\gamma_\mathrm{D}\left(m_{\mathrm{A}x}\sin\phi-m_{\mathrm{A}z}\cos\phi\right), & x\in(x_\mathrm{s};x_\mathrm{i}),\\ 0, & x\in[x_\mathrm{l};x_\mathrm{s}]\cup[x_\mathrm{i};x_\mathrm{r}].\end{cases} \tag{2.7}$$

The stationary solution for the amplitude and the wave number correspond to the case when

$$\frac{\partial\theta}{\partial t}=0,\quad \frac{\partial\phi}{\partial t}=-\omega, \tag{2.8}$$

where ω is the angular frequency of the wave and the time derivative of ϕ is negative due to section of $\vec{e}_y$ to be an axis around which $\vec{m}$ is precessing.

2.2 Small amplitude waves

For waves with small amplitude, Eqs. (2.4) and (2.5) can be linearised with respect to the amplitude, θ. Using Eq. (2.8), the following equations for stationary amplitude and

https://doi.org/10.4208/cicp.120615.090516a Published online by Cambridge University Press

wavenumber in the region without the damping, i.e. for $x\in[x_l;x_s]\cup[x_i;x_r]$, are obtained:

$$2\frac{d\theta}{dx}\frac{d\phi}{dx}+\frac{d^2\phi}{dx^2}\theta=0, \tag{2.9}$$

$$\frac{d^2\theta}{dx^2}-\left(\frac{d\phi}{dx}\right)^2\theta+\frac{\omega}{\beta_L}\theta=0. \tag{2.10}$$

It can be shown that the general solution of (2.9) and (2.10) is the following:

$$\theta^2=\sqrt{E^2+C^2}+E\sin(2\nu x+D), \tag{2.11}$$

$$\phi=\arctan\left(\frac{\sqrt{E^2+C^2}}{C}\tan\left(\nu x+\frac{D}{2}\right)+\frac{E}{C}\right)+F,\quad \nu=\sqrt{\frac{\omega}{\beta_L}}, \tag{2.12}$$

where C, D, E are constants that are obtained from the boundary conditions and F is a function[‡] that is independent of x. Hence, in general, the amplitude of the spin wave is not constant and has a periodic component, the scale of which depends on the boundary conditions. Since at $x=x_s$ the damping band begins, these oscillations in the amplitude are reflections from the damping zone and since the damping region was introduced as a part of a numerical method which provides the coupling between scales, the damping zone parameters should be selected such that these reflections remain small. In the case when a continuous sub-domain is considered, for example $x\in[x_l;x_s]$, it can be shown that

$$\begin{cases}\left.\frac{\partial\theta}{\partial x}\right|_{x=x_s}\le A,\\ \left.\frac{\partial^2\theta}{\partial x^2}\right|_{x=x_s}\le B\end{cases}\quad\Rightarrow\quad E\le\frac{2G+\sqrt{4G^2+16{\theta_0}^2\nu^2(\theta_0G+A^4)}}{8\theta_0\nu^2}, \tag{2.13}$$

where $G=4\theta_0A^2+\theta_0B^2+A^2B$ and θ_0 is the boundary condition for θ at $x=x_l$. Thus, if first and second derivative of the spin wave amplitude at the right boundary of the sub-domain is small ($A\to0$ and $B\to0$), then the oscillations in the amplitude inside the sub-domain are also small ($E\to0$). This means that the damping zone should be of the finite width, such that the spin waves are attenuated over relatively large region, thereby resulting in small values of spatial derivatives of the amplitude and leading to a small change of the solution in the region preceding the damping zone. Therefore the width of the damping zone depends on the prescribed accuracy. Moreover, small values of spatial derivatives of θ at the beginning of the damping zone can be achieved by selecting inhomogeneous damping strength, which starts from zero and increases towards the interface.

2.3 Damping of high frequency waves

In the region with damping, $x\in(x_s;x_i)$, for high frequency waves the average magnetisation vector is approaching a constant vector, provided that averaging region is sufficiently large. This can be seen when magnetisation vector, represented via angles θ and

[‡]From Eq. (2.8) it is seen that $F=-\omega t+F_1$, where F_1 is a constant.

https://doi.org/10.4208/cicp.120615.090516a Published online by Cambridge University Press

ϕ, see Eq. (2.3), has fast changing values of $\cos\phi$ and $\sin\phi$, which leads to the constant value of the average magnetisation, $\vec{m}_{\mathrm{A}}=\vec{e}_y$. Using this and the assumption of the amplitude being small, Eqs. (2.4) and (2.5) are linearised with respect to θ, which results in the following equations:

$$2\frac{\mathrm{d}\theta}{\mathrm{d}x}\frac{\mathrm{d}\phi}{\mathrm{d}x}+\frac{\mathrm{d}^2\phi}{\mathrm{d}x^2}\theta+\frac{\gamma_{\mathrm{D}}}{\beta_{\mathrm{L}}}\theta=0, \tag{2.14}$$

$$\frac{\mathrm{d}^2\theta}{\mathrm{d}x^2}-\left(\frac{\mathrm{d}\phi}{\mathrm{d}x}\right)^2\theta+\frac{\omega}{\beta_{\mathrm{L}}}\theta=0. \tag{2.15}$$

Note that compared to Eqs. (2.9) and (2.10), Eqs. (2.14) and (2.15) have only one additional term.

A particular solution of the system (2.14) and (2.15) can be obtained by taking $\phi=kx-\omega t$, which leads to

$$\theta=\theta_0\exp\left(\frac{-\gamma_{\mathrm{D}}}{2\beta_{\mathrm{L}}k}x\right),\quad k^2=\frac{\omega+\sqrt{\omega^2+{\gamma_{\mathrm{D}}}^2}}{2\beta_{\mathrm{L}}}. \tag{2.16}$$

For this particular solution, it can be observed that for high ω the decrease of the amplitude is small within the limited interval $x\in(x_{\mathrm{s}};x_{\mathrm{i}})$, i.e. high frequency waves are not damped efficiently[§]. Alternative explanation of this effect results from the group velocity of spin waves being dependent on the wave frequency and for the particular solution (2.16) the group velocity is the following:

$${v_{\mathrm{g}}}^2=8\beta_{\mathrm{L}}\frac{\omega^2+{\gamma_{\mathrm{D}}}^2}{\omega+\sqrt{\omega^2+{\gamma_{\mathrm{D}}}^2}}, \tag{2.17}$$

which means that high frequency waves move relatively fast through the damping band without being significantly affected. To avoid this effect, γ_{D} should be dependent on ω, which can be realised by the introduction of the dependency on time derivative of $\vec{m}$, which for the case of spin wave is the following:

$$\left|\frac{\partial}{\partial t}\vec{m}\right|=|\omega\sin\theta|, \tag{2.18}$$

assuming that stationary solution is considered, see Eq. (2.8). The details of the selection of the damping parameters are presented in the next section.

2.4 Damping band

As shown above, to avoid significant change of the spin wave amplitude in the region preceding the damping band, the amplitude should be attenuated slowly in the beginning of the damping region. This can be achieved by gradual increase of the damping

[§]Although here a particular solution is discussed, this can also be demonstrated numerically for the general case.

https://doi.org/10.4208/cicp.120615.090516a Published online by Cambridge University Press

strength. Moreover, the damping strength should be proportional to the angular frequency of the wave, such that high-frequency waves are subjected to stronger damping, which can be achieved by introduction of the dependence on the time derivative of $\vec{m}$. Taking this into account, the following expression for the damping strength is proposed:

$$\gamma_{\mathrm{D}} = g_{\mathrm{D}} (x - x_{\mathrm{s}})^2 \sqrt{\left| \frac{\partial}{\partial t} \vec{m} \right|}, \tag{2.19}$$

where g_{D} is a constant determining the damping strength and x_{s} is the coordinate of the beginning of the damping zone.

Within the damping band, magnetisation is damped to an average value $\vec{m}_{\mathrm{A}}$, which is calculated over a certain region. To obtain a normalised vector, such that $|\vec{m}_{\mathrm{A}}| = 1$, a non-normalised quantity $\vec{m}^*_{\mathrm{A}}$ is introduced at first. Its components are calculated in the following way:

$$m^*_{\mathrm{A}\nu} = a_\nu x^2 + b_\nu x + c_\nu, \quad \nu = \{x, y, z\}, \tag{2.20}$$

where coefficients a_ν, b_ν and c_ν are functions of x and are determined by fitting to the magnetisation $\vec{m}$ in the following way:

$$F_\nu (a_\nu, b_\nu, c_\nu, x) = \int_{x - s_{\mathrm{A}}/2}^{x + s_{\mathrm{A}}/2} \left(m_\nu (\zeta) - a_\nu \zeta^2 - b_\nu \zeta - c_\nu \right)^2 \mathrm{d}\zeta, \quad \nu = \{x, y, z\}, \tag{2.21}$$

$$(a_\nu, b_\nu, c_\nu) = \underset{a_\nu, b_\nu, c_\nu}{\operatorname{argmin}} F_\nu (a_\nu, b_\nu, c_\nu, x), \tag{2.22}$$

where $m_\nu (x)$ are components of $\vec{m}$. Thus for each x within the damping band, $\vec{m}^*_{\mathrm{A}}$ contains components that are points of the quadratic functions, which are fitted to the components of $\vec{m}$ in the interval of size s_{A} (averaging interval). In the discrete case such a fit becomes a weighted least square fit. Finally, $\vec{m}_{\mathrm{A}}$ is obtained by normalisation:

$$\vec{m}_{\mathrm{A}} = \frac{\vec{m}^*_{\mathrm{A}}}{|\vec{m}^*_{\mathrm{A}}|}. \tag{2.23}$$

3 Computational examples

In this section, at first, the stationary solution of the modified equations describing the system with the damping band in the case of one uniformly discretised domain is investigated. The influence of the damping band parameters on the solution is quantified. Following this, the domain is discretised piecewise-uniformly with two sub-domains: fine and coarse (see Fig. 1). At this step additional effects of interfacing domains with different mesh sizes is characterised. After that the case when initial conditions contain inhomogeneities, which create waves of multiple frequencies, is analysed. Finally, physical damping is introduced into the system to demonstrate limited range of high-frequency waves, which is the common reason for the increase in coarseness of spatial discretisation, and the ability of proposed method to handle these waves.

https://doi.org/10.4208/cicp.120615.090516a Published online by Cambridge University Press

In Section 3.1, a stationary example is considered, i.e. the computed quantities (amplitude and wavenumber) are time independent. Moreover the LLG equation is re-written in terms of angles (see (2.4) and (2.5)), therefore none of the numerical methods often used for the dynamic LLG equation [8] is required. The spatial derivatives are discretised using finite differences and the resulting system of non-linear equations is solved using the Newton-Raphson method. Starting from Section 3.2 the time-dependent solution is investigated and therefore a geometrical integration method for LLG equation is adopted. More details regarding the method including accuracy and stability can be found in [18].

Here multiscale examples with a sharp interface are considered, i.e. the interface between uniformly meshed domains with a different step size, which is intentionally created to localise the problem of wave reflection. Obviously, in the case of a mesh with gradually varying spatial step, waves with different wave lengths are reflected back at different locations. Thus such meshing requires a wider damping region if the contamination of the solution in the fine scale region is to be avoided. In order to illustrate effects from different scales clearly, the scale difference of one order of magnitude was selected for the examples in this section. The actual scale difference depends on the application of the multiscale method, i.e. the size of the features, which are to be represented on the coarse scale.

3.1 Amplitude-frequency

To investigate the behaviour of the system where the damping band is introduced, Eqs. (2.4) and (2.5) in the case of stationary solution (2.8) are solved numerically. The following boundary conditions are imposed:

$$\theta|_{x=x_\mathrm{l}}=\theta_0, \quad \phi|_{x=x_\mathrm{l}}=-\omega t+F_1; \tag{3.1}$$

$$\left.\frac{\mathrm{d}\theta}{\mathrm{d}x}\right|_{x=x_\mathrm{r}}=0, \quad \left.\frac{\mathrm{d}^2\phi}{\mathrm{d}x^2}\right|_{x=x_\mathrm{r}}=0. \tag{3.2}$$

In this particular example, the behaviour of the damping band region is investigated, therefore it is convenient to have constant amplitude and wavenumber in the region following the damping band, i.e. the right part of the domain (see Fig. 1). For a spin wave of a given frequency, equating derivatives of the amplitude and wavenumber to zero at the right boundary results in a constant solution in the adjoining region, which follows from the analytical solution, see Section 2.2. Thus boundary conditions in the form of (3.2) represent non-reflecting boundary conditions for the case when the solution is a spin wave. Note that such boundary conditions will not act as non-reflecting in the general case, since the superposition principle is not applicable to the solutions of the full LLG equation due to its non-linear nature. The initial phase, which is determined by the constant F_1, is taken to be 0.

To obtain a numerical solution for θ and ϕ, the domain $x_\mathrm{l}\le x\le x_\mathrm{r}$ is discretised into $N+1$ points, the spatial derivatives are approximated using sixth order finite differences

https://doi.org/10.4208/cicp.120615.090516a Published online by Cambridge University Press

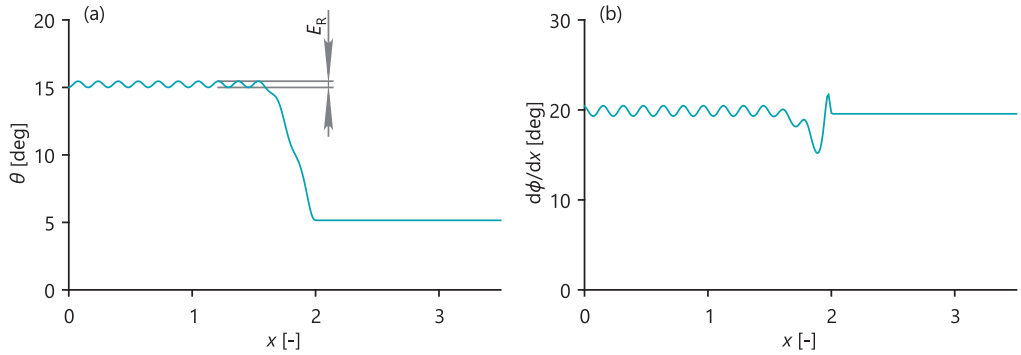


Figure 2: Spin wave amplitude (a) and wavenumber (b) for the case of $g_D = 10^3$, $s_A = 0.3$ and $\theta_0 = \pi/12$. The damping band is starting at $x_s = 1.5$ and has a width of $s = 0.5$. The scale of the oscillations of the amplitude, E_R, is marked in the figure.

(central finite differences are used inside the domain and forward/backward finite differences are used near the boundaries) and the integrals in (2.21) and (2.22) are calculated using the midpoint method. The solution of the discretised system is obtained using Newton-Raphson method. To ensure convergence, N is increased until solutions θ^C and θ^F with $(N+1)$ and $(N/0.7+1)$ discretisation points respectively do not differ by more than 1%, i.e. $\max\left|\theta^C - \theta^F\right|/\theta_0 < 0.01$.

The example of the solution for the amplitude and the wavenumber is shown in Fig. 2. Here $x_l = 0$, $x_r = 3.5$ and the damping zone starts at $x_s = 1.5$ and has a width of $s = 0.5$. As outlined in Section 2.4, the damping strength is quadratically increasing with x, therefore at x_s the amplitude is decreasing slowly. Within the damping band the solution is damped towards the average which is calculated in the window of size $s_A = 0.3$. As was shown in Section 2.2 for small amplitudes, in the domain without the damping the solution (the amplitude and the wavenumber) does contain periodic components, which depend on the boundary conditions. Spin waves are attenuated in the region $x_s \le x \le x_i$, thus for $x_l \le x \le x_s$ there are periodic changes in the amplitude, i.e. the solution to the left of the damping band is influenced by the reflections from the damping band. The wavenumber is influenced as well, however the largest change in wavenumber is observed within the damping band.

The influence of the damping band on the solution can be characterised by the dependence of the amplitude to the right of the damping band and the size of oscillations in the amplitude to the left of the damping band, E_R, on the frequency of the wave. In Fig. 3, these amplitude-frequency characteristics are illustrated, where the wave length of the non-damped wave,

$$\lambda = 2\pi\sqrt{\frac{\beta_L \cos\theta_0}{\omega}}, \tag{3.3}$$

is used as an argument on the horizontal axis, as opposed to the frequency. The damping band is seen to be acting as a low-pass filter, which attenuates waves with wave length that is lower than a certain "cut-off wave length", while waves with high wave lengths

https://doi.org/10.4208/cicp.120615.090516a Published online by Cambridge University Press

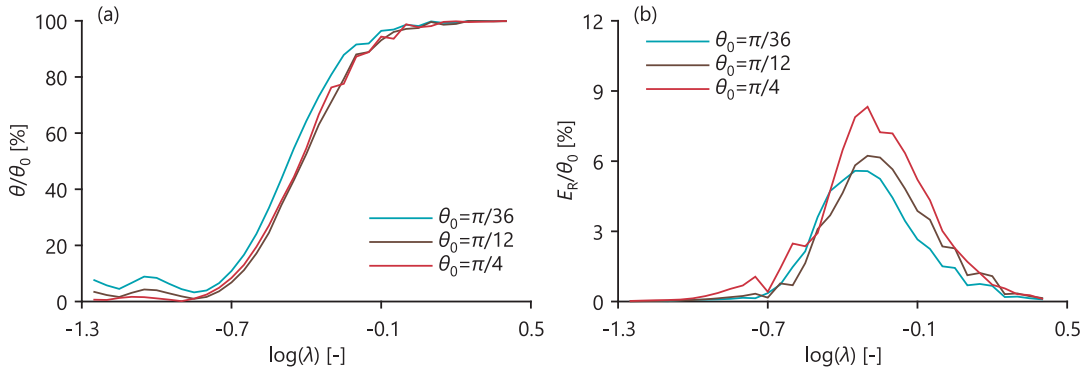


Figure 3: Dependence of spin wave amplitude to the right of the damping band, scaled by θ_0 (a), and the magnitude of the oscillations in the amplitude to the left of the damping band, E_R, scaled by θ_0 (b), on wave length for the case of $g_D = 10^3$, $s_A = 0.3$ and $s = 0.5$.

are unaffected by it. Although presence of the damping region creates perturbations in the amplitude to the left of it, the magnitude of these oscillations is negligibly small for both high and low wave lengths and is significant only in the region of the "cut-off wave length" (see Fig. 3). As was outlined in Section 2.2, these reflections depend on the size of the damping band, s, and decrease with increasing s.

In Figs. 3, 4 and 5, the influence of θ_0 (boundary condition amplitude), g_D (damping strength) and s_A (width of region in which $\vec{m}_A$ is calculated) respectively on the spin wave amplitude is shown. It is seen that the magnitude of the wave amplitude hardly influences the factor by which it is decreased by damping or the scale of the reflections from the damping band, see Fig. 3. There is only a small increase of the oscillations of the amplitude due to reflections for large θ_0. Therefore it can be concluded that the proposed damping method works efficiently for the spin waves with both small and large amplitudes.

As shown in Fig. 4, the damping strength (g_D) significantly influences the amplitude of spin waves with high frequency, while low frequency waves are not damped even for the case of high damping strength. The scale of the reflections is decreasing with damping strength. In Fig. 5, it is demonstrated that change of the width of region in which average magnetisation, $\vec{m}_A$, is calculated produces horizontal shift of the dependency of amplitude on the wave length and decrease of s_A leads to decrease of "cut-off wave length". Moreover, large values of s_A result in an increase of wave reflections from the damping region.

Non-smoothness of the dependencies in Figs. 3-5 is the result of the relation between the size of the domain in which the wave is propagating and the wave length. For example, for the small-amplitude waves, it can be seen that size of amplitude oscillations in the sub-domain without damping, E_R, depend on boundary conditions for the phase, ϕ, non-linearly, see Eq. (2.12), which in their turn depend on relation between size of the sub-domain and the wave length.

https://doi.org/10.4208/cicp.120615.090516a Published online by Cambridge University Press

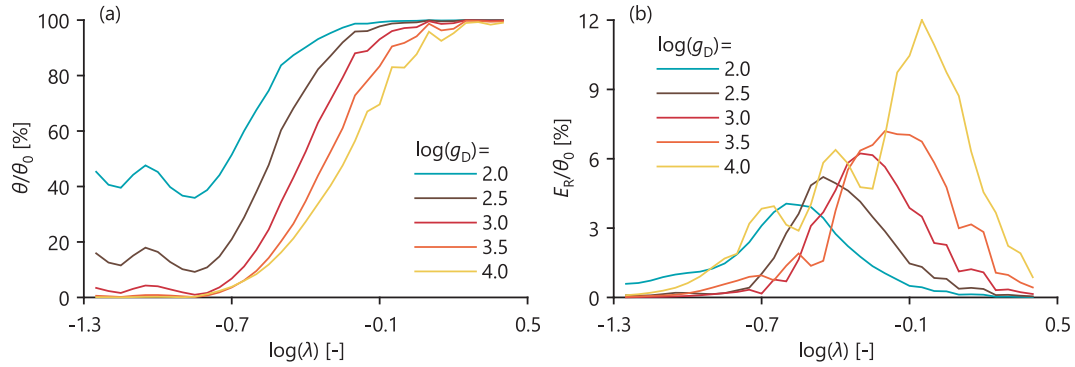


Figure 4: Dependence of spin wave amplitude to the right of the damping band, scaled by θ_0 (a), and magnitude of oscillations in the amplitude to the left of the damping band, scaled by θ_0 (b), on wave length for the case of $\theta_0=\pi/12$, $s_A=0.3$ and $s=0.5$.

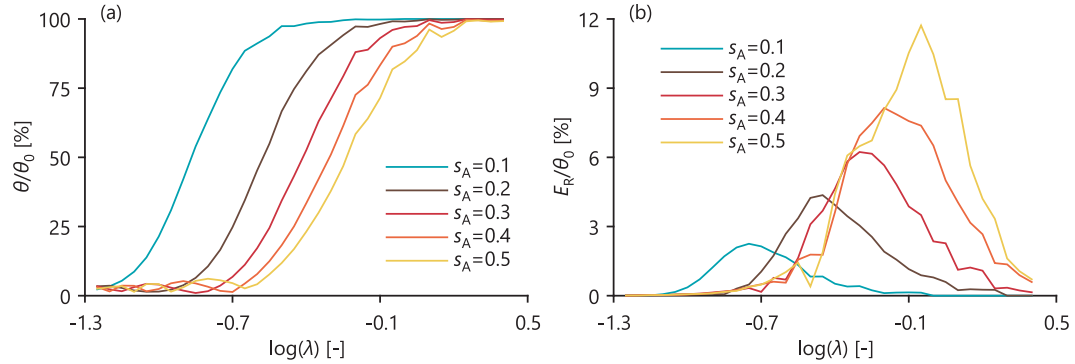


Figure 5: Dependence of spin wave amplitude to the right of the damping band, scaled by θ_0 (a), and magnitude of oscillations in the amplitude to the left of the damping band, scaled by θ_0 (b), on wave length for the case of $g_D=10^3$, $\theta_0=\pi/12$ and $s=0.5$.

3.2 Two length scales, spin waves

To investigate the case of inhomogeneous discretisation, a method of numerical solution of Eqs. (2.1) and (2.2) was implemented. Time-stepping was performed using mid-point method [18]. Second order central finite-difference method was used to spatially discretise the equations. The following initial and boundary conditions were used:

$$\vec{m}|_{x=x_l}=\vec{e}_x\sin\theta\cos\phi+\vec{e}_y\cos\theta+\vec{e}_z\sin\theta\sin\phi,\quad \phi=-\omega t, \tag{3.4}$$

$$\left.\frac{d\vec{m}}{dx}\right|_{x=x_r}=0, \tag{3.5}$$

$$\vec{m}|_{t=0}=\vec{e}_y, \tag{3.6}$$

where $\theta|_{t<T}=\theta_0 t/T$, $\theta|_{t\geq T}=\theta_0$ and $T=2\pi/\omega$. Moreover, to avoid reflections from the right boundary, an additional damping region was introduced, i.e. Eqs. (2.1) and (2.2)

https://doi.org/10.4208/cicp.120615.090516a Published online by Cambridge University Press

were modified further in the following way:

$$\frac{\partial}{\partial t}\vec{m} = -\beta_{\mathrm{L}}\vec{m}\times\frac{\partial^2}{\partial x^2}\vec{m} - \gamma_{\mathrm{b}}\vec{m}\times\left(\vec{m}\times\vec{e}_y\right), \quad \gamma_{\mathrm{b}} = \frac{g_{\mathrm{b}}\left(x-x_{\mathrm{b}}\right)^2}{\sqrt{2\pi T\beta_{\mathrm{L}}\cos\theta_0}}, \quad x\in[x_{\mathrm{b}};x_{\mathrm{r}}]. \tag{3.7}$$

Frequency-dependent damping, γ_{b}, was used. This region is effectively creating an absorbing boundary at $x = x_{\mathrm{b}}$ and it was introduced solely to avoid back-reflected waves. For the simulations $g_{\mathrm{b}} = 40$ was used.

The domain $0 \le x \le 4$ was split into two sub-domains with $0 \le x \le 2$ being a fine-scale domain having $\Delta x_{\mathrm{F}} = 1/160$ and $2 \le x \le 4$ being a coarse-scale domain having $\Delta x_{\mathrm{C}} = 1/16$. At the interface ($x_{\mathrm{i}} = 2$), the second derivatives were approximated using second order irregular grid central finite differences, which use three grid points: $(x_{\mathrm{i}} - \Delta x_{\mathrm{F}})$, x_{i} and $(x_{\mathrm{i}} + \Delta x_{\mathrm{C}})$. The damping band in the fine-scale domain starts at $x_{\mathrm{s}} = 1.5$ and ends at the interface. As was outlined above, there is an additional damping region starting at $x_{\mathrm{b}} = 2.5$ to absorb waves in the coarse-scale region. Fixed time step was used in the simulations, $\Delta t = T/48$. The spatial and time discretisations were selected based on the convergence study. The wave lengths that were used in the simulations ranged from $\lambda = 0.1$ to $\lambda = 1$. Thus waves with the highest wave length had sufficient resolution in the coarse scale region, while waves with the lowest wave length were resolved only in the fine scale region. The simulation was performed for $0 \le t \le 3t_{\mathrm{p}}$, where

$$t_{\mathrm{p}} = (x_{\mathrm{r}} - x_{\mathrm{l}})\sqrt{\frac{T}{8\pi\beta_{\mathrm{L}}\cos\theta_0}} \tag{3.8}$$

is the time required for the non-damped wave to propagate from x_{l} to x_{r}. After approximately $2t_{\mathrm{p}}$ the stationary solution is observed, i.e. amplitude and wavenumber are almost constant.

In Fig. 6, influence of the damping strength (g_{D}) and width of the averaging region (s_{A}) on the scale of the oscillations of the spin wave amplitude to the left of the damping band is shown. Values of E_{R} are averages calculated for $2t_{\mathrm{p}} \le t \le 3t_{\mathrm{p}}$. Compared to Figs. 4 and 5, it can be observed that for the case when the damping zone precedes the coarse scale, high-frequency spin waves should be sufficiently damped, otherwise wave reflections from the fine-coarse interface are observed. Therefore low damping strength or width of averaging region lead to large error due to non-damped waves that are reflected from the interface. High values of these parameters result in strong damping, which leads to the reflections from the damping zone. Optimal values for these parameters corresponding to the selected width of the damping zone, s, and difference between scales, can be found computationally.

In addition to the case when waves are generated in the fine scale region, a case of waves being generated in the coarse scale region was analysed. Only one wave length, $\lambda = 1$, was used, since only low frequency waves are well-resolved in the coarse scale. For this problem the absorbing boundary was moved to the left, i.e. modification (3.7) was

https://doi.org/10.4208/cicp.120615.090516a Published online by Cambridge University Press

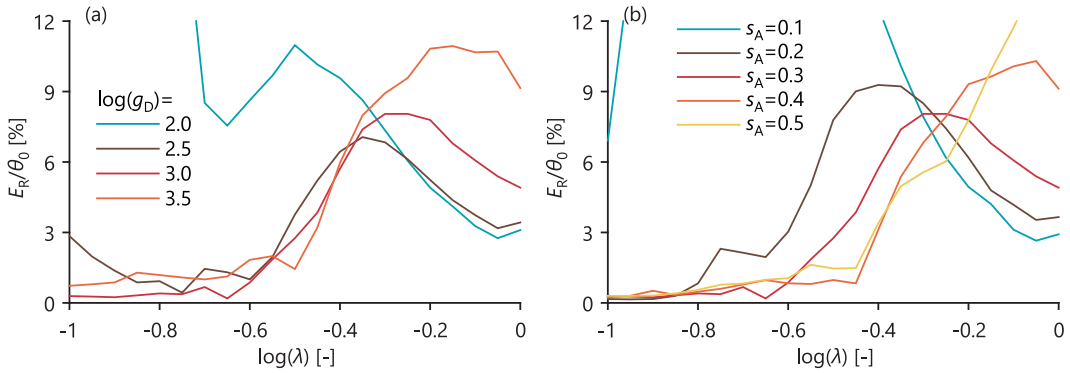


Figure 6: Magnitude of oscillations in the amplitude to the left of the damping band, scaled by θ_0. Average for $2t_p \le t \le 3t_p$ is taken. Variation of g_D with $s_A = 0.3$ (a) and variation of s_A with $g_D = 10^3$ (b) are shown. Other parameters are $\theta_0 = \pi/12$ and $s = 0.5$.

introduced for the region $x \in [x_l; x_b]$, where $x_b = 1.5$. It was observed that the reflections from the interface and the adjacent damping zone in the case when low frequency waves are propagating from the coarse into the fine region is almost the same as when waves are propagating from the fine into the coarse region. In the former case $E_R/\theta_0 = 5.5\%$ and in the latter case $E_R/\theta_0 = 4.9\%$ for the damping zone parameters $g_D = 10^3$ and $s_A = 0.5$ and the waves with the wave length of $\lambda = 1$.

3.3 Two length scales, inhomogeneous initial conditions

To validate the scale coupling, Eqs. (2.1) and (2.2) are solved with inhomogeneous initial conditions. In this section an additional absorbing zone in the region $x_b \le x \le x_r$ was not used. The following initial and boundary conditions were used:

$$\left.\frac{d\vec{m}}{dx}\right|_{x=x_l} = 0, \quad \left.\frac{d\vec{m}}{dx}\right|_{x=x_r} = 0, \quad \vec{m}|_{t=0} = \vec{e}_x \sin\psi + \vec{e}_y \cos\psi, \tag{3.9}$$

$$\psi = \begin{cases} \frac{\pi}{4}\cos^2\left(\frac{\pi}{2a}(x - x_p)\right), & |x - x_p| \le a, \\ 0, & |x - x_p| > a, \end{cases} \tag{3.10}$$

i.e. reflecting boundary conditions on both left and right boundaries were used. The initial inhomogeneity results in waves of various frequencies.

The same numerical method as in previous section is used here, as well as the same size of the domain and the same discretisation. The damping strength and the width of the averaging region were selected to be $g_D = 10^3$ and $s_A = 0.3$ respectively. Three different cases corresponding to the following initial conditions were analysed: inhomogeneity of the small scale, which creates high frequency waves that cannot propagate into coarse scale domain ($x_p = 1.45$, $a = 0.05$); inhomogeneity of the large scale ($x_p = 0$, $a = 0.5$); the intermediate case between the first and the second variants of the initial conditions ($x_p = 0$, $a = 0.2$). The time step was selected such that change (rotation) of $\vec{m}$ at any point and

https://doi.org/10.4208/cicp.120615.090516a Published online by Cambridge University Press

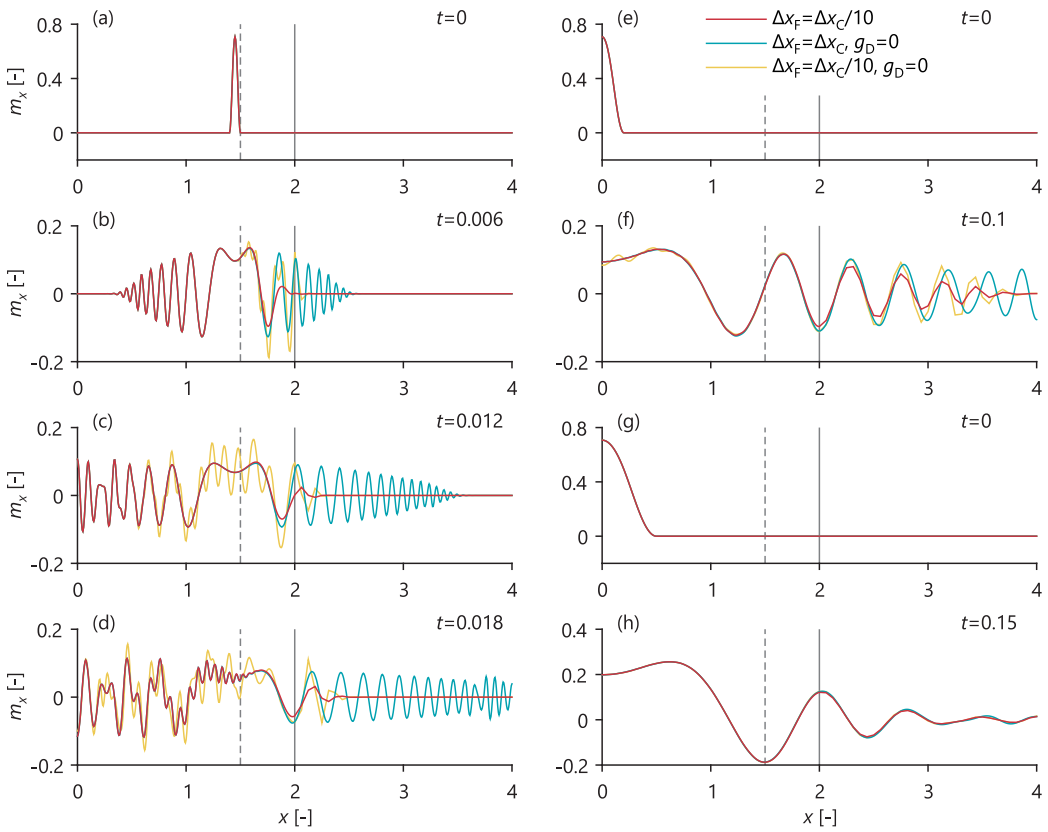


Figure 7: Evolution of x component of $\vec{m}$ with time in the domain with reflecting boundary conditions. Initial conditions contain inhomogeneities of size 0.05 (a-d), 0.2 (e-f) and 0.5 (g-h). Three cases are compared: fine-coarse discretisation with the damping band, fine scale in the entire domain without the damping band and fine-coarse discretisation without the damping band. Note that the vertical scale in figures is varied for better data representation.

during any time step is less than 7.5°. Results are shown in Fig. 7, where figures a-d correspond to small scale inhomogeneity, figures e-f correspond to the intermediate case and in figures g-h large scale inhomogeneity is shown. Moreover two additional cases where damping is absent ($g_D = 0$) are presented in Fig. 7: one with the same fine-coarse discretisation and one with uniformly discretised domain (fine-scale spatial discretisation), which is used as a reference solution. Results indicate that for any type of inhomogeneity in the initial conditions the solution in non-uniformly discretised domain with the damping band at the interface matches the solution in uniformly discretised domain in the region to the left of the damping band, i.e. no reflections from the interface are observed. The large-scale features propagate into the coarse scale, while small-scale features are damped. In the case when there is no damping band at the interface, components of m_x with high spacial frequency cannot get through the interface, since they cannot be represented on the coarse scale, and are reflected back to the fine scale thereby introducing an error in the fine-scale solution.

https://doi.org/10.4208/cicp.120615.090516a Published online by Cambridge University Press

Note that in order to evaluate the efficiency of the damping band, it is the fine scale region one should focus on. The course scale region is less relevant, since this region is designed to not be able to represent fine scale features. In Fig. 7 it is clear that simulations with a fine-coarse discretisation without the damping band (yellow curve) have unphysical oscillations to the left of the interface between the two regions. These oscillations are absent both in the simulations where the same fine scale was used throughout the simulation region (results that could be seen as numerically exact), as well as in the simulations with fine-coarse discretisation, when the here suggested damping technique is introduced.

3.4 Two length scales, spin waves and physical damping

To illustrate the advantages of domain separation into the coarse and the fine regions and applying damping at the interface, a realistic materials case, in which the physical damping is present, was considered. Here the standard physical (Gilbert) damping term [7] was added to the equations, resulting in the following system:

$$\frac{\partial}{\partial t}\vec{m} = -\beta_{\mathrm{L}}\vec{m}\times\frac{\partial^2}{\partial x^2}\vec{m} - \alpha_{\mathrm{L}}\vec{m}\times\left(\vec{m}\times\frac{\partial^2}{\partial x^2}\vec{m}\right) - \Gamma, \tag{3.11}$$

$$\Gamma = \begin{cases} \gamma_{\mathrm{D}}\vec{m}\times(\vec{m}\times\vec{m}_{\mathrm{A}}), & x\in(x_{\mathrm{s}};x_{\mathrm{i}}), \\ 0, & x\in[x_{\mathrm{l}};x_{\mathrm{s}}]\cup[x_{\mathrm{i}};x_{\mathrm{r}}]. \end{cases} \tag{3.12}$$

The physical damping (term containing α_{L}) is present in the entire domain while the numerical damping (term containing γ_{D}) is present only within the damping band at the interface. The same initial and boundary conditions as in Section 3.2 were used here, see Eqs. (3.4), (3.5) and (3.6), i.e. initially all magnetic moments are aligned with $\vec{e}_y$ and the spin wave excitation is driven at the left boundary. The absorbing zone was not used in these simulations, thus waves were reflected from the right boundary. For this example, the size of the coarse scale was extended, $x_{\mathrm{r}}=8$. The same time and spatial discretisation as in Section 3.2 was used. Physical damping parameter (α_{L}) was selected to be 0.01.

Two different frequencies were selected, which correspond to waves with wave lengths of $\lambda=0.1$ (Fig. 8), which cannot be resolved in the coarse scale, and $\lambda=1$ (Fig. 9), which is adequately represented at the coarse scale, see Eq. (3.3). Evolutions of spin wave amplitudes with time are shown in Figs. 8 and 9 for these two waves. Fine scale discretisation in the entire domain without the damping band provides the reference solution, where the wave freely propagates through the entire domain with decaying amplitude reaching the right boundary. Small transient oscillations in the amplitude due to initial excitation are present at the wavefront, as is clear e.g. in Fig. 8. Comparing Figs. 8 and 9 it can be observed that high frequency waves have a limited range, i.e. the decrease of the amplitude with x due to Gilbert damping is higher than of low frequency waves, thus they can be "cut off" by the introduction of the coarse scale. Note that since these are dispersive ways the low frequency wave travels slower and therefore the time scales

https://doi.org/10.4208/cicp.120615.090516a Published online by Cambridge University Press

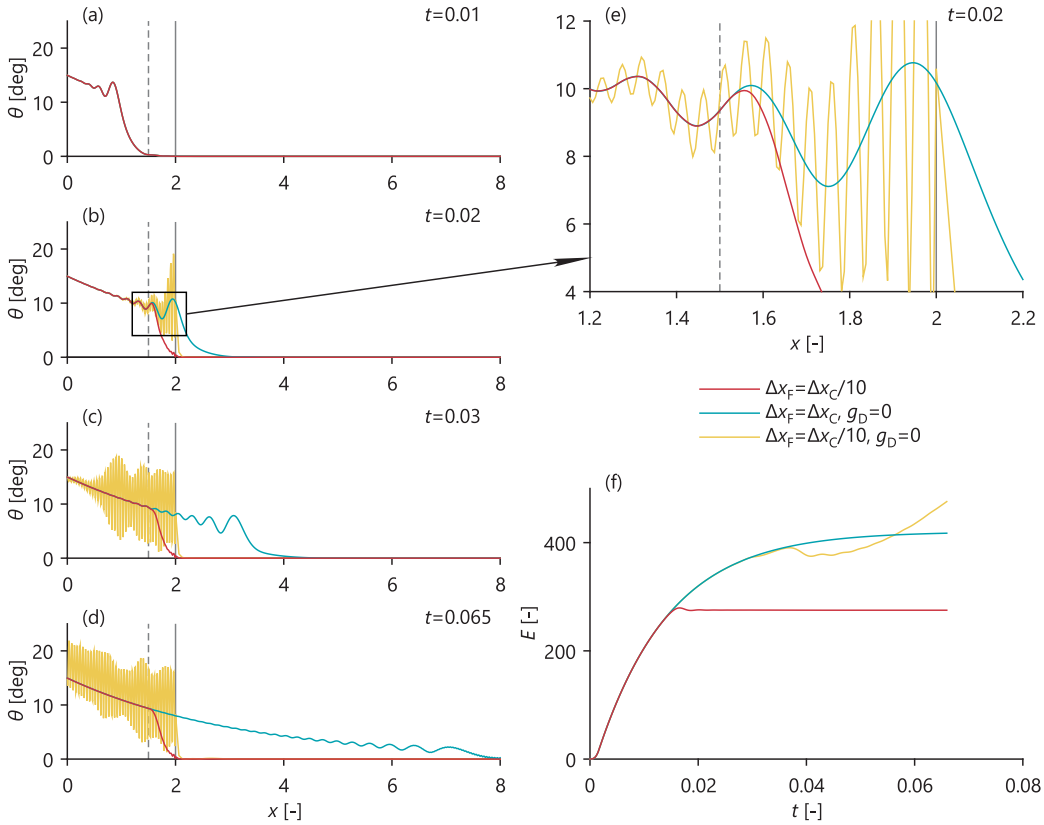


Figure 8: Evolution of spin wave amplitude with time in the domain with right reflecting boundary (a-e). Spin wave with a wave length $\lambda = 0.1$ is excited at the left boundary. Evolution of energy of the system with time (f). Three cases are compared: fine-coarse discretisation with the damping band (red), fine scale in the entire domain without the damping band (blue) and fine-coarse discretisation without the damping band (yellow).

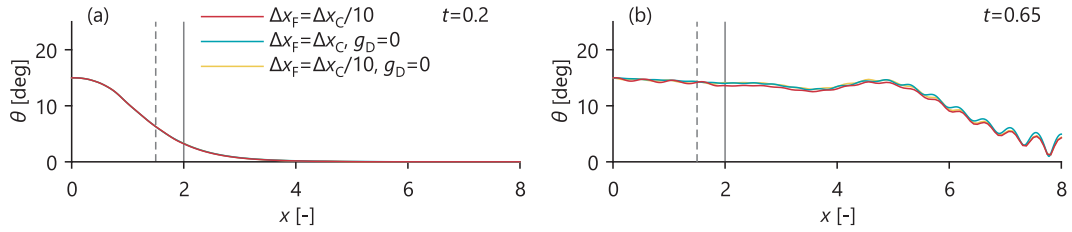


Figure 9: Evolution of spin wave amplitude with time in the domain with right reflecting boundary (a-b). Spin wave with a wave length $\lambda = 1$ is excited at the left boundary. Three cases are compared: fine-coarse discretisation with the damping band (red), fine scale in the entire domain without the damping band (blue) and fine-coarse discretisation without the damping band (yellow).

in Figs. 8 and 9 are not the same. When fine-coarse discretisation with an explicit interface between discretised areas and without the damping band at the interface is used, significant amount of wave reflections from the interface between the scales is observed

https://doi.org/10.4208/cicp.120615.090516a Published online by Cambridge University Press

for the high frequency waves, which is illustrated in Fig. 8. Because of the interference of the reflected components with the fine-scale solution, the solution is dominated by the numerical error and in this case the amplitude-frequency representation is not applicable. The presence of damping band does not affect the solution to the left of the damping region and completely attenuates high-frequency waves (Fig. 8) while not affecting low-frequency waves (Fig. 9).

By performing such damping of high frequency waves, the energy of the system, which is calculated as

$$E=\int_{x_1}^{x_r}\left(\left(\frac{\partial}{\partial x}m_x\right)^2+\left(\frac{\partial}{\partial x}m_y\right)^2+\left(\frac{\partial}{\partial x}m_z\right)^2\right)\mathrm{d}x, \tag{3.13}$$

is decreased as shown in Fig. 8f. The part of the wave, which in the undamped case is located to the right of the interface, does not contribute to the total energy when the damping band is considered[¶]. This should be taken into account for energy estimations in the systems with multiple scales. In the case without damping band and with multiple length scales, Fig. 8f shows that energy does not reach a steady state, due to instabilities of the solution caused by the boundary of fine and course scales.

4 Conclusions

In this article, a method establishing a transition between different scales, which are involved in modelling of magnetisation dynamics, was suggested. A way of introduction of a damping region in the proximity of the interface between two scales, which was originally proposed for coupling atomistic dynamics and finite-element regions in mechanics [12], is reformulated for the Landau-Lifshitz equation, which describes motion of the magnetic spins of atoms in its discrete form or behaviour of magnetisation as a vector field in its continuous form. This work is an initial step in realising multiscale modelling of magnetisation dynamics, by allowing course and fine grade simulations within the continuum model.

By using an example of small amplitude spin wave propagation in one-dimensional domain it was analytically shown that such damping zone at the interface should be of the finite width, which influences the amount of reflections from the interface and adjoining damping region. The increase of the width of the damping zone leads to the decrease of wave reflections, i.e. waves should be attenuated gradually. For the same reason, non-constant damping strength, which starts from zero at the beginning of the damping zone, further minimises wave reflections. Moreover, the dispersive nature of the spin waves requires the introduction of the dependence of the damping strength on wave frequency, which is technically realised by using the time derivative of the magnetisation.

Computational examples of spin wave propagation were used to study the efficiency of the introduced modification of the Landau-Lifshitz equation. It was shown that for

[¶]Numerically integral in (3.13) was calculated by trapezoidal rule.

https://doi.org/10.4208/cicp.120615.090516a Published online by Cambridge University Press

particular width of the damping zone and particular difference in scales there are optimal values for the parameters of the damping zone, which minimise the scale of wave reflections from the interface and the damping band. This is a critical step in performing multiscale modelling of magnetisation dynamics and allows for seamless connection between different length-scales in such simulations.

The ultimate objective of the proposed method is to absorb waves at the atomistic/continuum interface in the case of dynamic material behaviour, although all the analysis in the current article was performed for the coupling of fine scale and coarse scale continuum descriptions. A natural extension, outside the scope of the current study, would be to replace fine scale continuum with the atomistic spin dynamics, where the material behaviour is represented by the set of atomistic LLG equations (instead of the PDE) where unknowns are the magnetic moments of the discrete set of atoms (instead of the vector field) and the sum over neighbours is used instead of the spatial derivatives, for details see [9].

The proposed method should be also valid in 2D and 3D cases, however preliminary data suggests it would have a lower efficiency due to the existence of the waves with a propagation direction not parallel to the interface normal. Since it was demonstrated that the efficiency of the proposed damping method depends on the width of the damping band, in higher dimensions, a wider damping band is required to achieve the same efficiency as in 1D case. A more detailed investigation of the current methodology for higher dimensions is underway.

Acknowledgments

The authors would like to acknowledge the support of eSSENCE. The authors would also like to acknowledge the support from the Swedish Research Council (VR) and the KAW foundation (projects 2013.0020 and 2012.0031).

References

[1] E. Beaurepaire, J.-C. Merle, A. Daunois, and J.-Y. Bigot. Ultrafast spin dynamics in ferromagnetic nickel. *Physical Review Letters*, 76(22):4250–4253, 1996.

[2] J. Stöhr, M. G. Samant, J. Lüning, A. C. Callegari, P. Chaudhari, J. P. Doyle, J. A. Lacey, S. A. Lien, S. Purushothaman, and J. L. Speidell. Liquid crystal alignment on carbonaceous surfaces with orientational order. *Science*, 292(5525):2299–2302, 2001.

[3] T. Gerrits, H. A. M. van den Berg, J. Hohlfeld, L. Bär, and T. Rasing. Ultrafast precessional magnetization reversal by picosecond magnetic field pulse shaping. *Nature*, 418(6897):509–512, 2002.

[4] A. V. Kimel, A. Kirilyuk, A. Tsvetkov, R. V. Pisarev, and T. Rasing. Laser-induced ultrafast spin reorientation in the antiferromagnet $TmFeO_3$. *Nature*, 429(6994):850–853, 2004.

[5] I. Tudosa, C. Stamm, A. B. Kashuba, F. King, H. C. Siegmann, J. Stöhr, G. Ju, B. Lu, and D. Weller. The ultimate speed of magnetic switching in granular recording media. *Nature*, 428(6985):831–833, 2004.

https://doi.org/10.4208/cicp.120615.090516a Published online by Cambridge University Press

[6] I. Radu, K. Vahaplar, C. Stamm, T. Kachel, N. Pontius, H. A. Dürr, T. A. Ostler, J. Barker, R. F. L. Evans, R. W. Chantrell, A. Tsukamoto, A. Itoh, A. Kirilyuk, T. Rasing, and A. V. Kimel. Transient ferromagnetic-like state mediating ultrafast reversal of antiferromagnetically coupled spins. *Nature*, 472(7342):205–208, 2011.
[7] A. Aharoni. *Introduction to the theory of ferromagnetism*. Oxford University Press, 1996.
[8] I. Cimrák. A survey on the numerics and computations for the Landau-Lifshitz equation of micromagnetism. *Archives of Computational Methods in Engineering*, 15(3):277–309, 2008.
[9] B. Skubic, J. Hellsvik, L. Nordström, and O. Eriksson. A method for atomistic spin dynamics simulations: implementation and examples. *Journal of Physics: Condensed Matter*, 20(31):315203, 2008.
[10] E. B. Tadmor and R. E. Miller. *Modeling materials*. Cambridge University Press, 2011.
[11] R. E. Miller and E. B. Tadmor. A unified framework and performance benchmark of fourteen multiscale atomistic/continuum coupling methods. *Modelling and Simulation in Materials Science and Engineering*, 17(5):053001, 2009.
[12] S. Qu, V. Shastry, W. A. Curtin, and R. E. Miller. A finite-temperature dynamic coupled atomistic/discrete dislocation method. *Modelling and Simulation in Materials Science and Engineering*, 13(7):1101–1118, 2005.
[13] B. Shiari, R. E. Miller, and D. D. Klug. Multiscale simulation of material removal processes at the nanoscale. *Journal of the Mechanics and Physics of Solids*, 55(11):2384–2405, 2007.
[14] N. Kazantseva, D. Hinzke, U. Nowak, R. W. Chantrell, U. Atxitia, and O. Chubykalo-Fesenko. Towards multiscale modeling of magnetic materials: simulations of FePt. *Physical Review B*, 77(18):184428, 2008.
[15] T. Jourdan, A. Marty, and F. Lançon. Multiscale method for Heisenberg spin simulations. *Physical Review B*, 77(22):224428, 2008.
[16] C. Andreas, A. Kákay, and R. Hertel. Multiscale and multimodel simulation of Bloch-point dynamics. *Physical Review B*, 89(13):134403, 2014.
[17] S. Bartels and A. Prohl. Convergence of an implicit finite element method for the Landau-Lifshitz-Gilbert equation. *Siam Journal On Numerical Analysis*, 44(4):1405–1419, 2006.
[18] M. d'Aquino, C. Serpico, and G. Miano. Geometrical integration of Landau-Lifshitz-Gilbert equation based on the mid-point rule. *Journal of Computational Physics*, 209(2):730–753, 2005.

https://doi.org/10.4208/cicp.120615.090516a Published online by Cambridge University Press